Mesoscopic model for diffusion-influenced reaction dynamics

Kay Tucci[a)]
Max-Planck-Institut für Physik Komplexer Systeme, Nöthnitzer Strasse 38, 01187 Dresden, Germany and SUMA-CeSiMo, Universidad de Los Andes, Mérida 5101, Venezuela

Raymond Kapral[b)]
Max-Planck-Institut für Physik Komplexer Systeme, Nöthnitzer Strasse 38, 01187 Dresden, Germany and Chemical Physics Theory Group, Department of Chemistry, University of Toronto, Toronto, ON M5S 3H6, Canada

(Received 2 December 2003; accepted 4 February 2004)

A hybrid mesoscopic multiparticle collision model is used to study diffusion-influenced reaction kinetics. The mesoscopic particle dynamics conserves mass, momentum, and energy so that hydrodynamic effects are fully taken into account. Reactive and nonreactive interactions with catalytic solute particles are described by full molecular dynamics. Results are presented for large-scale, three-dimensional simulations to study the influence of diffusion on the rate constants of the $A+C \rightleftharpoons B+C$ reaction. In the limit of a dilute solution of catalytic C particles, the simulation results are compared with diffusion equation approaches for both the irreversible and reversible reaction cases. Simulation results for systems where the volume fraction ϕ of catalytic spheres is high are also presented, and collective interactions among reactions on catalytic spheres that introduce volume fraction dependence in the rate constants are studied. © *2004 American Institute of Physics.* [DOI: 10.1063/1.1690244]

I. INTRODUCTION

The dynamics of large complex systems often occurs on disparate time and space scales. A direct molecular dynamics simulation of the equations of motion for such systems is difficult because of this scale separation and the large numbers of molecules such systems may contain. Consequently, mesoscopic models play an important role in investigations of the dynamics of these systems.

The use of Langevin and Fokker–Planck equations for Brownian motion is well known[1,2] and these models have been used in much wider contexts—for example, in investigations of reaction dynamics in the condensed phase.[3] Such stochastic models are useful when it is impossible or inappropriate to simulate the full dynamics of the system, including all solvent degrees of freedom.

Suspensions of colloidal particles are also often treated using mesoscopic models of various types. While the dynamics of the colloidal particles may be accurately modeled using Langevin dynamics, hydrodynamic interactions play an important role in dense colloidal suspensions. The friction tensors that enter the Langevin equations depend on the colloidal particle configuration. To compute the frictional properties of dense suspensions, the intervening solvent is often approximated by the continuum equations of hydrodynamics to determine the hydrodynamic interactions among the colloidal particles.

Other approaches for constructing mesoscopic dynamics of complex systems include construction of effective solvent models to be used in the context of full molecular dynamics simulations.[4] Such models allow one to investigate systems of high complexity that cannot be studied by straightforward molecular dynamics simulation schemes.

In this article we show how diffusion-influenced reactions can be studied using a multiparticle mesoscopic dynamics.[5,6] In this dynamical scheme, particle positions and velocities are continuous variables and the dynamics consists of free-streaming and multiparticle collisions. Multiparticle collisions are carried out by partitioning the system into cells and performing a specific type of random rotation of the particle velocities in each cell that conserves mass, momentum, and energy. The hydrodynamic equations are obtained on long-distance and -time scales[6] and the model permits efficient simulation of hydrodynamic flows.[6,7] Since the dynamics is carried out at the particle level, it is straightforward to construct hybrid schemes where solute molecules that undergo full molecular dynamics are embedded in the mesoscopic solvent.[8] Hydrodynamic interactions among solute particles are automatically accounted for in the multiparticle mesoscopic dynamics.[9] The method has been generalized to treat phase-segregating fluids with surfactants.[10]

Diffusion-influenced reaction dynamics is widely used to model processes like enzymatic turnover or collision-induced isomerization in complex systems. von Smoluchowski constructed a continuum theory for such reactions based on a solution of the diffusion equation.[11] In this article we focus on the reversible $A+C \rightleftharpoons B+C$ reaction where a considerable body of research has been concerned with the development of refined theoretical models.[12–18] Simulation schemes[19–22] for three-dimensional diffusive reaction dynamics have been constructed. Diffusion-influenced reactions taking place in a dense field of catalytic particles are strongly affected by perturbations of the diffusion field aris-

[a)]Electronic mail: kay@ula.ve
[b)]Electronic mail: rkapral@chem.utoronto.ca

ing from reactions at the different catalytic sites.[23–29] This effect is similar to the hydrodynamic interactions that enter colloidal suspension dynamics. We show how collective effects on diffusion-influenced reaction dynamics can be studied by simulations of a mesoscopic model for these systems. The mesoscopic multiparticle collision model allows us to simulate systems with tens of millions of particles for long times in order to determine power-law decays and nonanalytic catalytic particle density effects on the reaction rates.

The outline of the paper is as follows. Section II sketches the mesoscopic multiparticle collision model and presents its generalization to multicomponent systems. The evolution equations that encode the multiparticle mesoscopic dynamics are presented in Sec. III. The computation of the diffusion coefficient, a necessary ingredient for the analysis of reaction dynamics, is given in Sec. IV. In Sec. V we show how the model can be generalized to treat chemical reactions. In particular, we study the reaction $A+C \rightleftharpoons B+C$, which occurs upon collision with catalytic C particles. The simulation algorithms and simulation results for dilute and concentrated suspensions of catalytic spheres are presented in Sec. VI. The conclusions of the investigation are contained in Sec. VII.

II. MULTICOMPONENT MESOSCOPIC MULTIPARTICLE DYNAMICS

The mesoscopic dynamics we consider comprises two steps: multiparticle collisions among the particles and free streaming between collisions.[6] Suppose the system contains N particles with positions and velocities given by $(\mathbf{X}^{(N)},\mathbf{V}^{(N)})=(\mathbf{x}_1,\ldots,\mathbf{x}_N,\mathbf{v}_1,\ldots,\mathbf{v}_N)$. While the particle positions and velocities are continuous variables, for the purpose of effecting collisions, the system is divided into L cells labeled by the index ξ. Collisions occur locally in the cells in the following way: Rotation operators $\hat{\omega}$, chosen randomly from a set of rotation operators $\Omega=\{\hat{\omega}_1,\ldots,\hat{\omega}_k\}$, are assigned to each cell ξ of the system. If a cell ξ contains n_ξ particles at time t and the center-of-mass velocity in the cell is $\mathsf{V}_\xi(t)=n_\xi^{-1}\Sigma_{i=1}^{n_\xi}\mathbf{v}_i(t)$, the post-collision values of the velocities of the particles in the cell, $\mathbf{v}_i^*$, are computed by rotating the particle velocities relative to V_ξ and adding V_ξ to the result

$$\mathbf{v}_i^*(t)=\mathsf{V}_\xi(t)+\hat{\omega}_\xi[\mathbf{v}_i(t)-\mathsf{V}_\xi(t)]. \tag{1}$$

After the collision events in each cell, the particles free stream to their new positions at time $t+\tau$:

$$\mathbf{x}_i(t+\tau)=\mathbf{x}_i(t)+\mathbf{v}_i^*(t)\tau. \tag{2}$$

This simple dynamics has been shown to conserve mass, momentum, and energy. The exact hydrodynamic equations are obtained on macroscopic scales, and the system relaxes to an equilibrium Boltzmann distribution of velocities.[6] Consequently, the dynamics, although highly idealized, has correct behavior on macroscopic scales which are long compared to the effective collision times in the model. Since the dynamics is described at the particle level, it is a simple matter to couple this mesoscopic dynamics to the full molecular dynamics of solute species embedded in it.[8,30] The model is similar in spirit to the direct simulation Monte Carlo model,[31] but with a different discrete-time collision dynamics that simplifies the simulations and makes them more efficient.

The mesoscopic dynamics for a multicomponent system can be carried out in a similar way by generalizing the multiparticle collision rule. Suppose the N-particle system comprises different species $\alpha=A,B,\ldots$ with masses m_α. In this case it is useful to introduce the function Θ_i^α that characterizes the species α of a given particle i. This function has the following properties:

$$\Theta_i^\alpha\Theta_i^{\alpha'}=\delta_{\alpha\alpha'}; \tag{3}$$

i.e., particle i cannot be of different species at the same time. Also,

$$\sum_\alpha \Theta_i^\alpha=1, \tag{4}$$

so that particle i has to have some species type. The number of particles of species α is given by

$$N_\alpha=\sum_{i=1}^{N}\Theta_i^\alpha. \tag{5}$$

There are many ways in which the multiparticle collision rule can be generalized for systems with several species, and we consider one version that is consistent with the requirement that mass, momentum, and energy be conserved. Let $\mathsf{V}_\xi^{(\alpha)}$ be the center-of-mass velocity of particles of species α that are in the cell ξ at time t:

$$\mathsf{V}_\xi^{(\alpha)}(t)=\frac{1}{n_\xi^{(\alpha)}(t)}\sum_{i|\mathbf{x}\in\mathcal{V}}\Theta_i^\alpha\mathbf{v}_i(t), \tag{6}$$

where $n_\xi^{(\alpha)}$ is the number of particles of the species α in cell ξ with volume $\mathcal{V}$ at time t. The center-of-mass velocity of all $n_\xi(t)=\Sigma_\alpha n_\xi^{(\alpha)}(t)$ particles in the cell ξ at time t is given by

$$\mathsf{V}_\xi(t)=\frac{\Sigma_\alpha n_\xi^{(\alpha)}m_\alpha\mathsf{V}_\xi^{(\alpha)}(t)}{\Sigma_\alpha n_\xi^{(\alpha)}m_\alpha}. \tag{7}$$

In the model we adopt, two different types of multiparticle collisions occur. The first is a collision that involves particles of all species. To perform this collision, we use a rotation operator $\hat{\omega}$, which is applied to every particle in a cell as for single-component system. The second type of multiparticle collision involves only particles of the same species. The rotation operator $\hat{\omega}^\alpha$ effects this collision and is applied to each particle of species α in the cell. Not only does it change from cell to cell and with time like $\hat{\omega}$, but it also changes from species to species.

The multiparticle collision process can be divided into these two independent steps. For the set of particles that are in the cell ξ, first we perform the all-species collision as

$$\mathbf{v}_i''=\mathsf{V}_\xi+\hat{\omega}_\xi(\mathbf{v}_i-\mathsf{V}_\xi), \tag{8}$$

where $\mathbf{v}_i$ is the precollision velocity of the particle i and $\mathbf{v}_i''$ is the velocity after this step. Second, we apply the one-species rotation operator

$$\mathbf{v}_i^* = \sum_\alpha \Theta_i^\alpha (\mathsf{V}_\xi''^{(\alpha)} + \hat{\omega}_\xi^\alpha (\mathbf{v}_i'' - \mathsf{V}_\xi''^{(\alpha)})), \tag{9}$$

where $\mathsf{V}_\xi''^{(\alpha)}$ is the center-of-mass velocity of particles of species α after the all-species collision step. Note that $\hat{\omega}_\xi$ is applied to all particles in the cell, but the $\hat{\omega}_\xi^\alpha$ are applied only on particles of species α.

From Eqs. (8) and (9) the post-collision velocity of a particle may be expressed as

$$\mathbf{v}_i^* = \mathsf{V}_\xi + \hat{\omega}_\xi (\Theta_i^\alpha \mathsf{V}_\xi^{(\alpha)} - \mathsf{V}_\xi) + \sum_\alpha \Theta_i^\alpha (\hat{\omega}_\xi^\alpha \hat{\omega}_\xi (\mathbf{v}_i - \mathsf{V}_\xi^{(\alpha)})). \tag{10}$$

III. EVOLUTION EQUATIONS

The dynamics described above can be encoded in an evolution equation for the phase space probability density:

$$\mathsf{P}(\mathbf{V}^{(N)}, \mathbf{X}^{(N)} + \mathbf{V}^{(N)}\tau, t+\tau) = e^{\mathsf{L}_0 \tau} \mathsf{P}(\mathbf{V}^{(N)}, \mathbf{X}^{(N)}, t+\tau) = \hat{\mathcal{C}} \mathsf{P}(\mathbf{V}^{(N)}, \mathbf{X}^{(N)}, t), \tag{11}$$

where the free-streaming Liouville operator is

$$\mathsf{L}_0 = \sum_\alpha \sum_{i=1}^N \Theta_i^\alpha (\mathbf{v}_i \cdot \boldsymbol{\nabla}_i), \tag{12}$$

and $N = \Sigma_\alpha N_\alpha$ is the total number of particles in the system. If we choose the rotation operators $\hat{\omega}$ and $\hat{\omega}^\alpha$ randomly from the set Ω, the collision operator may be written as

$$\hat{\mathcal{C}} \mathsf{P}(\mathbf{V}^{(N)}, \mathbf{X}^{(N)}, t) = \frac{1}{\|\Omega\|^L} \sum_{\Omega^L} \int d\mathbf{V}'^{(N)} P(\mathbf{V}'^{(N)}, \mathbf{X}^{(N)}, t) \times \prod_\alpha \prod_{i=1}^N \Theta_i^\alpha \delta(\mathbf{v}_i - \mathsf{V}_\xi' - \hat{\omega}_\xi (\mathsf{V}_\xi'^{(\alpha)} - \mathsf{V}_\xi') - \hat{\omega}_\xi^\alpha \hat{\omega}_\xi (\mathbf{v}_i' - \mathsf{V}_\xi'^{(\alpha)})), \tag{13}$$

where L is the number of cells.

We may write the evolution equation in continuous time by introducing a δ-function collision term which accounts for the fact that the multiparticle collisions occur at discrete time intervals. We have

$$\frac{\partial}{\partial t} P(\mathbf{V}^{(N)}, \mathbf{X}^{(N)}, t) = (-\mathsf{L}_0 + \mathcal{C}) P(\mathbf{V}^{(N)}, \mathbf{X}^{(N)}, t), \tag{14}$$

where the collision operator $\mathcal{C}$ acts on the velocities of the particles at discrete times $m\tau$ and is defined as

$$\mathcal{C} P(\mathbf{V}^{(N)}, \mathbf{X}^{(N)}, t) = \sum_{m=0}^\infty \delta(t - m\tau)(\hat{\mathcal{C}} - 1) P(\mathbf{V}^{(n)}, \mathbf{X}^{(N)}, t). \tag{15}$$

If Eq. (14) is integrated over a time interval $m\tau - \epsilon$ to $(m+1)\tau - \epsilon$, we recover Eq. (11) corresponding to multiparticle collisions followed by free streaming. Instead, integration over the jump at $t = (m+1)\tau$ yields an analogous discrete time equation with free streaming followed by collision.

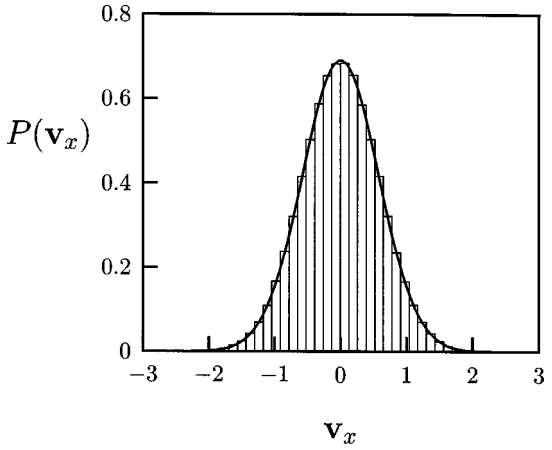

FIG. 1. Comparison of the simulated velocity distribution (histogram) with the Maxwell–Boltzmann distribution function (solid line) for $k_B T = 1/3$.

Assuming that the system is ergodic, then, in view of the conservation of mass, momentum, and energy, the stationary distribution of the Markov chain in Eq. (11) is given by the microcanonical ensemble expression

$$P_0(\mathbf{V}^{(N)}, \mathbf{X}^{(N)}) = \mathcal{N} \delta\left(\frac{1}{2N} \sum_{i=1}^N \sum_\alpha \Theta_i^\alpha m^\alpha \|\mathbf{v}_i\|^2 - \frac{d}{2\beta} \right) \times \delta\left(\sum_{i=1}^N \sum_\alpha \Theta_i^\alpha m^\alpha (\mathbf{v}_i - \overline{\mathbf{v}}) \right), \tag{16}$$

where $\overline{\mathbf{v}}$ is the mean velocity of the system, d is the dimension, and $\mathcal{N}$ is a normalization constant. If we integrate P_0 over the phase space of all particles except particle i, we obtain the Maxwell–Boltzmann distribution in the limit of large N.

Figure 1 shows the results of a simulation of the velocity probability distribution for a system with volume $V = 100^3$ cells of unit length and $N = 10^7$ particles. The particles were initially uniformly distributed in the volume V and all particles had the same speed $|\mathbf{v}| = 1$, but different random directions. To obtain the results in this figure we assumed that the species were mechanically identical with mass $m = 1$ and used the multiparticle collision rule in Eq. (10) with rotations $\hat{\omega}_\xi$ and $\hat{\omega}_\xi^\alpha$ selected from the set $\Omega = \{\pi/2, -\pi/2\}$ about axes whose directions were chosen uniformly on the surface of a sphere ($\pm\pi/2$ collision rule). This version of the collision rule for mechanically identical particles will be used in all calculations presented in this paper.

The figure compares the histogram of the x component of the velocity with the Maxwell–Boltzmann distribution

$$P_m(v_x) = \left(\frac{m\beta}{2\pi} \right)^{1/2} e^{-\beta m v_x^2/2}, \tag{17}$$

where $\beta = (k_B T)^{-1}$, and confirms that this initial distribution evolves to the Maxwell–Boltzmann distribution under mesoscopic dynamics.

We may also write an evolution equation for any dynamical variable $a(\mathbf{V}^{(N)}, \mathbf{X}^{(N)})$ as

$$\frac{d}{dt} a(\mathbf{V}^{(N)}, \mathbf{X}^{(N)}, t) = (\mathsf{L}_0 + \mathsf{C}) a(\mathbf{V}^{(N)}, \mathbf{X}^{(N)}, t), \tag{18}$$

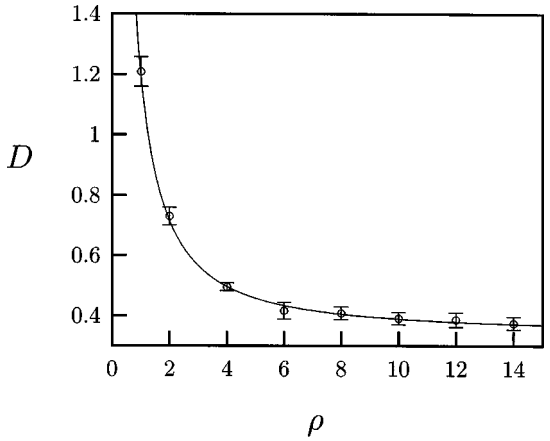

FIG. 2. Comparison of the simulated diffusion coefficient (⊙) with the Boltzmann value (solid line). The $\pm\pi/2$ collision rule was used to obtain the results. The volume was $V=100^3$ and the temperature was $k_BT=1/3$.

where C has the same form as $\mathcal{C}$ in Eq. (15) with $\hat{\mathcal{C}}$ replaced by $\hat{\mathsf{C}}$:

$$\hat{\mathsf{C}}a(\mathbf{V}^{(N)},\mathbf{X}^{(N)},t) = \frac{1}{\|\Omega\|^L}\sum_{\Omega^L}\int d\mathbf{V}'^{(N)}a(\mathbf{V}'^{(N)},\mathbf{X}^{(N)},t)\prod_{\alpha}\prod_{i=1}^{N}\Theta_i^{\alpha} \times\delta(\mathbf{v}_i'-\mathsf{V}_\xi-\hat{\omega}_\xi(\mathsf{V}_\xi^{(\alpha)}-\mathsf{V}_\xi)-\hat{\omega}_\xi^{\alpha}\hat{\omega}_\xi(\mathbf{v}_i-\mathsf{V}_\xi^{(\alpha)})). \quad (19)$$

This equation is the starting point for the generalization to reacting systems in Sec. V.

IV. DIFFUSION

Knowledge of the value of the diffusion coefficient is essential for the analysis of diffusion-influenced reaction kinetics. In this section we determine the diffusion coefficient as a function of the density from simulations of the mesoscopic multiparticle dynamics and derive an approximate analytical expression for its value.

The diffusion coefficient is given by the time integral of the velocity correlation function. For the discrete time dynamics of the model, the time integral is replaced by its trapezoidal rule approximation, as shown by a discrete-time Green–Kubo analysis.[8,30] Thus the diffusion coefficient D is given by

$$D=\frac{1}{2}\langle v_x v_x\rangle+\sum_{\ell=1}^{\infty}\langle v_x v_x(\ell\tau)\rangle, \quad (20)$$

where v_x is the x component of the velocity of a tagged particle in the system. (We suppress the species index α for the case of mechanically identical particles since all species have the same diffusion coefficient.) We have computed D using this expression as well as the formula for D in terms of the mean-square displacement as a function of the mean particle density per cell, ρ. The results are shown in Fig. 2.

An approximate expression for D can be derived by assuming a single relaxation time approximation. If we suppose the decay is given by a single relaxation time, we have

$$\frac{\langle v_x v_x(\ell\tau)\rangle}{\langle v_x v_x\rangle}\approx\left(\frac{\langle v_x v_x(\tau)\rangle}{\langle v_x v_x\rangle}\right)^{\ell}\equiv(r_D)^{\ell}. \quad (21)$$

The diffusion coefficient is then approximately given by

$$D\approx-\frac{1}{2}(v_x v_x)+\langle v_x v_x\rangle\sum_{\ell=0}^{\infty}r_D^{\ell}=\frac{\langle v_x v_x\rangle(1+r_D)}{2(1-r_D)}. \quad (22)$$

The relaxation rate may be computed in the Boltzmann approximation:[6]

$$\langle v_{1x}v_{1x}(\tau)\rangle=\int d\mathbf{v}\,v_{1x}\sum_{\omega}\sum_{n=1}^{\infty}\frac{\rho^n}{\|\Omega\|n!}e^{-\rho} \times\int d\mathbf{v}^{(n)}\delta(\mathbf{v}-\mathbf{v}_1)\prod_{i=1}^{n}\phi(\mathbf{v}_i)\sum_{j=1}^{n}v_{jx}^*, \quad (23)$$

where v_{1x} is the x component velocity of the single particle 1. Since cross correlations between different particles are not present for self-diffusion, we have

$$\langle v_{1x}v_{1x}(\tau)\rangle=\frac{1}{\|\Omega\|}\sum_{\omega}\sum_{n=1}^{\infty}\frac{\rho^n e^{-\rho}}{n!}\int d\mathbf{v}^{(n)}v_{1x}v_{1x}^*\prod_{i=1}^{n}\phi(\mathbf{v}_i). \quad (24)$$

The x component of the post-collision velocity v_{1x}^* may be written using Eq. (10) for the $\pm\pi/2$ collision rule discussed above as

$$v_{1x}^*=\frac{1}{4\pi}\int d\hat{n}\{\mathsf{V}_x+\hat{n}_x[\hat{n}\cdot(\mathsf{V}^{(\alpha)}-\mathsf{V})]\} +\frac{1}{(4\pi)^2}\int d\hat{n}^{(\alpha)}\int d\hat{n}\hat{n}_x^{(\alpha)}(\hat{n}^{(\alpha)}\cdot\hat{n}) \times[\hat{n}\cdot(\mathbf{v}_1-\mathsf{V}^{(\alpha)})], \quad (25)$$

where $\hat{n}$ and $\hat{n}^{(\alpha)}$ are the normal vectors associated with the rotation operators $\hat{\omega}$ and $\hat{\omega}^{\alpha}$, respectively. As a result of this integration we obtain

$$v_{1x}^*=\frac{1}{3}(v_{1x}+2\mathsf{V}_x). \quad (26)$$

Assuming that particles of different species have the same mass and substituting Eq. (26) into Eq. (24), we find

$$\langle v_{1x}v_{1x}(\tau)\rangle=\sum_{n=1}^{\infty}\frac{\rho^n e^{-\rho}}{n!}\int d\mathbf{v}_1(v_{1x})^2\left(\frac{n+2}{3n}\right)\phi(\mathbf{v}_1) =\frac{\langle v_{1x}v_{1x}\rangle}{3}\sum_{n=1}^{\infty}\frac{\rho^n e^{-\rho}}{n!}\left(\frac{2}{n}+1\right). \quad (27)$$

For large enough ρ, we may approximate this expression by

$$\langle v_{1x}v_{1x}(\tau)\rangle\approx\frac{\langle v_{1x}v_{1x}\rangle}{3}\sum_{n=1}^{\infty}\frac{\rho^n e^{-\rho}}{n!}(2+n), \quad (28)$$

which yields

$$r_D=\frac{2(1-e^{-\rho})+\rho}{3\rho}. \tag{29}$$

Substituting r_D into Eq. (22), the expression for the diffusion coefficient is

$$D=\frac{k_bT}{2m}\left(\frac{2\rho+1-e^{-\rho}}{\rho-1+e^{-\rho}}\right). \tag{30}$$

This analytic formula is compared with the simulation results in Fig. 2 where it is seen that it provides an excellent approximation to the simulation results over all of the physically interesting density range.

V. REACTIVE DYNAMICS

Next, we consider a reactive system with M finite-sized catalytic spherical particles (C) and a total of $N=N_A+N_B$ A and B particles which react with the C particles through the reactions

$$A+C\underset{k_r}{\overset{k_f}{\rightleftharpoons}}B+C. \tag{31}$$

The A and B particles undergo both nonreactive and reactive collisions with C and the multiparticle collisions described in Sec. II among themselves. The macroscopic mass action rate law may be written as

$$\frac{d}{dt}\delta\overline{n_A}(t)=-(k_f+k_r)\delta\overline{n_A}(t)\equiv-k\delta\overline{n_A}(t), \tag{32}$$

where $\delta\overline{n_A}(t)=\overline{n_A}(t)-\overline{n}_A^{\rm eq}$ is the deviation of mean number density of A particles from its equilibrium value and $k=k_f+k_r$ is the reciprocal of the chemical relaxation time. We have incorporated the fixed number density of the catalytic C particles into the rate constants.

The microscopic evolution equation for this system may be written by simply augmenting the free-streaming evolution operator in Eq. (12) with a Liouville operator L that describes the interactions of the A and B particles with the C particles. If the interactions of A and B with C are through continuous potentials, L takes the standard form $\mathsf{L}=\mathbf{F}\cdot\boldsymbol{\nabla}_{\mathbf{P}}$, where $\mathbf{F}$ is the force between the A and B particles and C and $\mathbf{P}$ is the vector of the momenta of the particles.

For the purposes of calculation and illustration, we adopt a model where the C particles are fixed in space and have radius σ. The A and B particles either bounce back from the catalytic spheres without changing their identity or react with probability p_R. In this case the evolution equation for any dynamical variable in the system is given by

$$\frac{d}{dt}a(\mathbf{X})(N),\mathbf{V}^{(N)},t)=(\mathsf{L}_0\pm\mathsf{L}_\pm+\mathsf{C})a(\mathbf{X}^{(N)},\mathbf{V}^{(N)},t), \tag{33}$$

where the $\pm$ signs apply for $t>0$ and $t<0$, respectively. The Liouville operators $\mathsf{L}_\pm$ describing the reactive and nonreactive collisions with the catalytic particles are given by

$$\mathsf{L}_\pm=\sum_\alpha\sum_{j=1}^{M}\sum_{i=1}^{N}|\mathbf{v}_i\cdot\hat{\mathbf{r}}_{ij}|\,\theta(\mp\mathbf{v}_i\cdot\hat{\mathbf{r}}_{ij})\,\delta(r_{ij}-\sigma)\times(\hat{b}_{ij}-1)\Theta_i^\alpha+p_R\sum_\alpha\sum_{j=1}^{M}\sum_{i=1}^{N}|\mathbf{v}_i\cdot\hat{\mathbf{r}}_{ij}|\,\theta(\mp\mathbf{v}_i\cdot\hat{\mathbf{r}}_{ij})\times\delta(r_{ij}-\sigma)\hat{b}_{ij}(\gamma\mathcal{P}^{\alpha\alpha'}-1)\Theta_i^\alpha. \tag{34}$$

Here $\hat{\mathbf{r}}_{ij}=(\mathbf{x}_i-\mathbf{x}_j)/r_{ij}$ is a unit vector along the line of centers between particle i and the catalytic sphere j, $r_{ij}=|\mathbf{x}_i-\mathbf{x}_j|$ is the magnitude of this vector, and the operator $\hat{b}_{ij}$ converts the velocity of particle i to its post-collision value after collision with the catalytic sphere j:

$$\hat{b}_{ij}(\mathbf{v}_1,\mathbf{v}_2,\ldots,\mathbf{v}_i,\ldots,\mathbf{v}_N)=(\mathbf{v}_1,\mathbf{v}_2,\ldots,\mathbf{v}_i^*,\ldots,\mathbf{v}_N). \tag{35}$$

For bounce-back dynamics we have $\mathbf{v}_i^*=-\mathbf{v}_i$. The operator $\mathcal{P}^{\alpha\alpha'}$ acts on the species labels to effect reactive collisions so that $\mathcal{P}^{\alpha\alpha'}\Theta_i^\alpha=\Theta_i^{\alpha'}$, where $\alpha'=B$ if $\alpha=A$ and vice versa. The factor γ accounts for the possibility that the forward and reverse reactions occur with different probabilities, leading to an equilibrium constant $K_{\rm eq}=\gamma^{-1}$, which is different from unity.

Rate law

The chemical rate law for this system my be derived by taking the dynamical variable a to be the deviation of the number of particles of species A from its average value $\chi=N_A-\langle N_A\rangle=\delta N_A=-\delta N_B$, where

$$N_A=\sum_{i=1}^{N}\Theta_i^A. \tag{36}$$

The angular brackets $\langle\cdots\rangle$ signify an average over an equilibrium ensemble where the numbers of A and B molecules fluctuate, but their sum is fixed, $N_A+N_B=N$. Starting with Eq. (33) for $t>0$ and using standard projection operator methods,[32] we may write a generalized Langevin equation for $\chi(t)$ in the form

$$\frac{d}{dt}\chi(t)=f_\chi(t)-\frac{\langle(\mathsf{L}_-\chi)\chi\rangle}{\langle\chi\chi\rangle}\chi(t)-\int_0^t dt'\frac{\langle(\mathsf{L}_-\chi)e^{\mathcal{Q}\mathsf{L}_+t'}\mathcal{Q}\mathsf{L}_+\chi\rangle}{\langle\chi\chi\rangle}\chi(t-t'), \tag{37}$$

where we have introduced the projection operator $\mathcal{P}a=\langle a\chi\rangle\langle\chi\chi\rangle^{-1}\chi$ and its complement $\mathcal{Q}=1-\mathcal{P}$. The random force is $f_\chi(t)=\exp[\mathcal{Q}\mathsf{L}_+t]\mathcal{Q}\mathsf{L}_+\chi$.

Averaging this equation over a nonequilibrium ensemble where χ does not fluctuate yields the generalized chemical rate law

$$\frac{d}{dt}\overline{\delta n_A}(t)=-\frac{\langle(\mathsf{L}_-\chi)\chi\rangle}{\langle\chi\chi\rangle}\overline{\delta n_A}(t)-\int_0^t dt'\frac{\langle(\mathsf{L}_-\chi)e^{\mathcal{Q}\mathsf{L}_+t'}\mathcal{Q}\mathsf{L}_+\chi\rangle}{\langle\chi\chi\rangle}\overline{\delta n_A}(t-t'). \tag{38}$$

The contribution

$$\frac{\langle(\mathsf{L}_-\chi)\chi\rangle}{\langle\chi\chi\rangle}=k_{0f}(1+K_{\rm eq}^{-1}) \tag{39}$$

determines the initial rate arising from direct collisions of the A and B particles with the catalytic spheres. For bounce-back collision dynamics of the A and B species with the catalytic sphere C, we have

$$k_{0f}=p_R\sigma^2\left(\frac{8\pi k_BT}{m}\right)^{1/2}n_C, \tag{40}$$

where n_C is the constant number density of catalytic spheres. The memory term accounts for all diffusion-influenced effects arising from recollisions with the catalytic spheres.

VI. RESULTS

A. Simulation method

The simulation of the model is carried out in a cubic box with sides L_B and periodic boundary conditions. The centers of the spheres of radius σ are located in this box, taking care to preserve periodic conditions on the edges when the spheres lie partially outside the cube. Once the catalytic spheres are placed in the box, the initial positions of the particles are assigned values that are within the cube, but outside the spheres. The velocities are chosen from a Maxwell–Boltzmann distribution.

Given the initial distribution of particles and particle velocities, the simulation begins by grouping the particles in cubic cells of size 1 within which the multiparticle collision operators act to change the velocities of all particles, preserving their positions. Then the displacement of each particle is computed using the post-collision velocity, taking into account the periodic boundary conditions of the cube and the bound-back collisions with the spheres. When a particle hits a sphere it may react with probability p_R, and the sign of its velocity is changed. Collisions between particles and spheres occur in continuous time in the interval $[t,t+\tau]$. When many catalytic spheres are present a particle may hit several spheres in one unit time τ.

Once all the particles have been moved, the time advances one unit τ and the particles are regrouped to apply the multiparticle collision rule again.

B. Single catalytic sphere

In order to test the utility of the mesoscopic model we investigate a system that contains a dilute distribution of independent catalytic C particles so that the dynamics may be described by considering a single C particle (labeled 1) with radius σ in a medium of A and B particles. In the case where A particles are converted irreversibly to B upon collision with C the chemical rate law takes the form $d\overline{n}_A(t)/dt=-k_f(t)\overline{n}_A(t)$, where $k_f(t)$ is the time-dependent rate coefficient. If the dynamics of the A density field may be described by a diffusion equation, we have the standard partially absorbing sink problem first considered by von Smoluchowski.[11] To determine the rate constant we must solve the diffusion equation

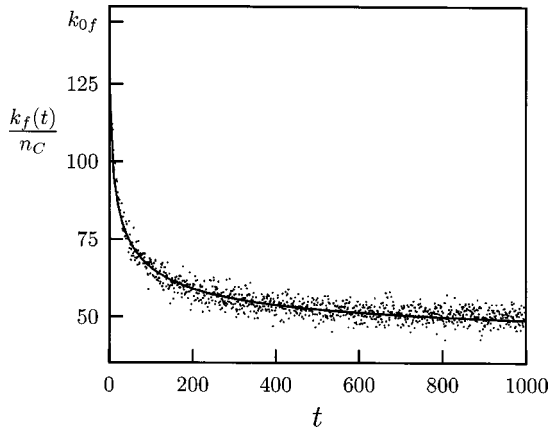

FIG. 3. Plot of the time dependent rate constant $k_f(t)/n_C$ vs t for $\sigma=10$. The solid line is theoretical value of $k_f(t)$ using Eq. (43) and $\overline{\sigma}=\sigma+1$.

$$\frac{\partial n_A(\mathbf{r},t)}{\partial t}=D_An_A(\mathbf{r},t), \tag{41}$$

subject to the boundary condition[33]

$$4\pi D\overline{\sigma}^2\hat{\mathbf{r}}\cdot(\boldsymbol{\nabla}n_A)(\hat{\mathbf{r}}\overline{\sigma},t)=k_{0f}n_A(\hat{\mathbf{r}}\sigma,t). \tag{42}$$

This equation assumes that the continuum diffusion equation is valid up to $\overline{\sigma}>\sigma$, which accounts for the presence of a boundary layer in the vicinity of the sphere surface where the continuum diffusion description should fail. The resulting expression for the time-dependent rate coefficient is[34]

$$k_f(t)=\frac{k_{0f}k_D}{k_{0f}+k_D}+\frac{k_{0f}^2}{k_{0f}+k_D}\exp\left[\left(1+\frac{k_{0f}}{k_D}\right)^2\frac{D}{\overline{\sigma}^2}t\right]\times\operatorname{erfc}\left[\left(1+\frac{k_{0f}}{k_D}\right)\left(\frac{Dt}{\overline{\sigma}^2}\right)^{1/2}\right]. \tag{43}$$

Here $k_D=4\pi\overline{\sigma}D$ is the rate constant for a diffusion-controlled reaction for a perfectly absorbing sphere.

The time-dependent rate coefficient $k_f(t)$ may be determined directly from the simulation by monitoring the A species density field and computing $-[d\overline{n}_A(t)/dt]/\overline{n}_A(t)$. The results of such a computation for irreversible reaction ($\gamma=0$) with probability $p_R=0.5$ are shown in Fig. 3.

The system size is 100^3 volume units and there is a sphere of radius $\sigma=10$ located in the center of the system. The simulation starts with $N(0)=N_A(0)=10^7$ particles of species A with unit mass uniformly distributed in the space. The initial velocities are Maxwell distributed with $k_BT/m=1/3$. The time-dependent rate coefficient starts at k_{0f} and decays to its asymptotic value k_f. In our mesoscopic model the continuum theory cannot apply on the scale of one multiparticle collision cell, so we have taken $\overline{\sigma}=\sigma+1$ to approximately account for the microscopic boundary layer. One sees good agreement between the simulation and diffusion theory results.

In Fig. 4(a) we plot the values of k_f extracted from the simulation data in this way versus the radius of the catalytic sphere.

The figure shows the increasing importance of diffusion-influenced effects on the value of the rate constant as σ in-

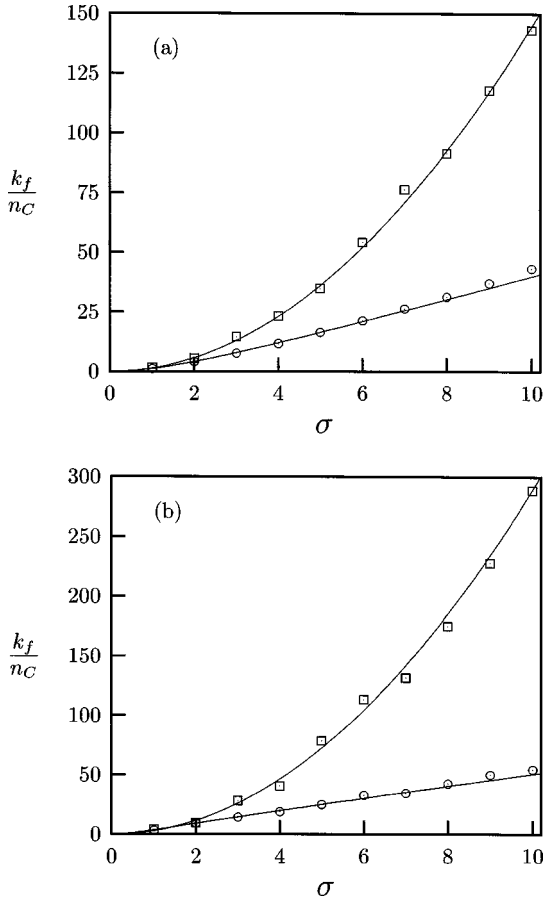

FIG. 4. Plot of k_f/n_C ($\odot$) vs σ, the radius of the catalytic sphere. The initial value $k_f(t=0)=k_{0f}$ ($\boxdot$) is also plotted versus σ in this figure. The solid lines are the theoretical values of these quantities determined from $k^{-1}=[k_{0f}(1+K_{\rm eq}^{-1})]^{-1}+k_D^{-1}$. (a) Irreversible reaction ($K_{\rm eq}^{-1}=0$) with $p_R=0.5$. (b) Reversible reaction ($K_{\rm eq}^{-1}=1$) with $p_R=1$.

creases. While k_{0f} grows quadratically with σ in accordance with Eq. (40), we see that k_f grows more slowly and approaches the diffusion-limited value of k_D, which depends linearly on σ for large σ. The theoretical estimate $k_f^{-1}=k_{0f}^{-1}+k_D^{-1}$ is in good agreement with the simulation results.

A similar calculation can be carried out for the reversible case ($\gamma=1$ and $p_R=1$). For reversible reactions the chemical relaxation rate $k(t)$ is given by Eq. (43) with k_{0f} replaced by $k_0=k_{0f}+k_{0r}=k_{0f}(1+K_{\rm eq}^{-1})$ and, therefore, $k^{-1}=k_0^{-1}+k_D^{-1}$ (Ref. 12). For our simulation conditions $K_{\rm eq}=1$ so that $k_0=2k_{0f}$. Also $k_f=k_r$. In Fig. 4(b) we plot the simulation values of k_f for the reversible reaction and compare them with the diffusion equation formula. Once again, good agreement is found. The effects of diffusion appear at somewhat smaller values of σ since k_0 is larger for the reversible reaction and the diffusion-limited value of the rate constant is reached at smaller values of σ.

C. Random distribution of catalytic spheres

If instead of a single catalytic sphere we have a random distribution of M spheres of radius σ in the volume V, the rate constant will depend in a nontrivial way on the catalytic sphere density or volume fraction $\phi=4\pi\sigma^3M/(3V)$. The reactions at one sphere surface will alter the A and B particle density fields there. From the perspective of a continuum diffusion equation approach, since the diffusion Green function which couples the dynamics at the different spheres is long ranged, the interactions from many catalytic spheres determine the value of the rate constant. The problem is analogous to the long-range interactions that determine hydrodynamic effects on the many-particle friction coefficient. There have been a number of studies of the volume fraction dependence of the rate constant.[12,23–28] These derivations rely on resummations of classes of interactions among the reacting spheres or other techniques.

The chemical relaxation rate for a system with a random distribution of catalytic spheres with volume fraction ϕ is given by[12,23,24]

$$k(\phi)=k\left[1+\left(\frac{(k_{0f}+k_{0r})^3}{(k_{0f}+k_{0r}+k_D)^3}3\phi\right)^{1/2}+\cdots\right], \tag{44}$$

where, as earlier, $k^{-1}=(k_{0f}+k_{0r})^{-1}+k_D^{-1}$. The first finite-density correction to the rate constant depends on the square root of the volume fraction. This nonanalytic volume fraction dependence arises from the fact that the diffusion Green function acts like a screened Coulomb potential coupling the diffusion fields around the catalytic spheres. As in the Debye theory of electrolytes, one must sum an infinite series of divergent terms to obtain the nonanalytic ϕ dependence.

The mesoscopic multiparticle collision dynamics follows the motions of all of the reacting species and their interactions with the catalytic spheres. Consequently, all many-sphere collective effects are automatically incorporated in the dynamics. We have carried out simulations of the chemical relaxation rate constant $k(\phi)$ as a function of the volume fraction of the catalytic spheres for a reversible reaction with $\gamma=1$ ($K_{\rm eq}^{-1}=1$) and $p_R=0.25$ as well as an irreversible reaction with $\gamma=0$ ($K_{\rm eq}^{-1}=0$) and $p_R=0.5$. For this choice of parameters the theoretical formula predicts that $k(\phi)$ for the reversible reaction is equal to $k_f(\phi)$ for the irreversible reaction. Our simulations were performed for systems with a volume fraction ϕ of catalytic spheres with radius $\sigma=3$ in a system of size 100^3 multiparticle cells and an initial number density of A particles, $n_A(0)=10$ per cell. The results shown in Fig. 5 were obtained from an average over five realizations of the random distribution of catalytic spheres.

We see that the simulation results confirm the existence of a $\phi^{1/2}$ dependence on the volume fraction for small volume fractions. As predicted by the theory for the chosen parameter values, the reversible and irreversible data overlap, even in the high-volume-fraction regime.

For larger volume fractions the results deviate from the predictions of Eq. (44) and the rate constant depends strongly on the volume fraction. An expression for the rate constant that includes higher-order corrections has been derived for the irreversible case[23] and takes the following form:

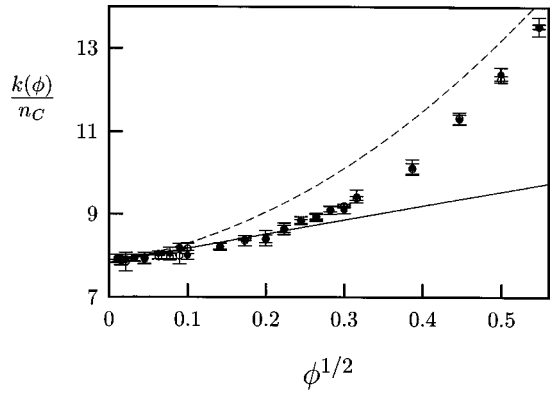

FIG. 5. Relaxation rate coefficient $k(\phi)/n_C$ as a function of the square root of the volume fraction $\phi^{1/2}$ for $\sigma=3$ and $k_BT=1/3$. Irreversible reaction $k_f(\phi)$ (●). Reversible reaction $k(\phi)$ (⊙). For some values of ϕ the two cases cannot be distinguished in the figure because the data points overlap. The solid line is determined using Eq. (44). The dashed line is obtained using Eq. (45) which includes higher-order corrections in the volume fraction.

$$k(\phi)=k\Bigg\{1+(3\phi\kappa^3)^{1/2}+3\phi\kappa^3\Bigg[\ln[(3\phi\kappa^3)^{1/2}]+1 -2(\kappa^{-1}-\kappa^{-2})+\gamma_E+\ln(2+4\kappa) +J\left(2\kappa^{-1},\frac{k_{0f}+2k_D}{k_{0f}-k_D}\kappa^3\right)\Bigg]+\cdots\Bigg\}, \tag{45}$$

where $\gamma_E=0.57721...$ is the Euler constant, $\kappa=k_{0f}/(k_{0f}+k_D)$, and

$$J(A,B)=\int_A^\infty du\,\frac{u^3}{(u+1)^2(Bu^3+2)}. \tag{46}$$

The dashed line in Fig. 5 is the value of $k(\phi)/n_C$ given by Eq. (45). We see that this formula describes the departure from the $\phi^{1/2}$ behavior that is seen in Fig. 5; however, the deviation from the $\phi^{1/2}$ form occurs at smaller ϕ values than indicated by the simulation results. The formula does not provide a quantitative estimate of the rate constant at high volume fractions, as might be expected in view of its series character.

From these results we conclude that the mesoscopic multiparticle collision dynamics provides a powerful tool for the exploration of concentration effects on diffusion-influenced reaction kinetics. Such concentration dependence is often difficult to explore by other means.

VII. CONCLUSION

We have demonstrated that large-scale simulations of diffusion-influenced reaction kinetics are possible by using the mesoscopic multiparticle collision model. With this model the dynamics of tens of millions of particles interacting with hundreds of catalytic spheres could be followed for long times to obtain the rate constants characterizing the population decay. Such simulations would be very costly using full molecular dynamics methods.

Since the dynamics is followed at the (mesoscopic) particle level, a number of noteworthy features of the dynamical scheme are worth mentioning. From a technical point of view the dynamics is stable and no difficulties like those associated with discretizations of the diffusion equation or boundary conditions arise. Reversible and irreversible reaction kinetics may be treated in similar fashion. All details of interactions arising from competition among the catalytic spheres in a dense suspension are automatically taken into account; thus, screening effects enter naturally in the dynamics.

The model may be generalized to any reaction scheme and is not restricted to the simple $A+C\rightleftharpoons B+C$ reaction with catalytic C particles discussed in this paper. Since solute molecules embedded in the mesoscopic solvent evolve by full molecular dynamics (without solvent–solvent interactions), the model will be most efficient when solvent–solvent interactions are a major time-limiting factor in the simulation. This could be case for conformational changes of large molecules in solution, reactions involving energy transfer in solution, etc. Thus, the model should find applicability in a variety of circumstances when diffusion-influenced reaction kinetics is important.

ACKNOWLEDGMENT

This work was supported in part by a grant from the Natural Sciences and Engineering Research Council of Canada.

[1] S. Chandrasekhar, Rev. Mod. Phys. **15**, 1 (1943).
[2] C. W. Gardiner, *Handbook of Stochastic Methods*, 2nd ed. (Springer, New York, 2002).
[3] P. Hänggi, P. Talkner, and M. Borkovec, Rev. Mod. Phys. **62**, 251 (1990).
[4] See S. O. Nielsen and M. L. Klein, in *Bridging the Time Scales: Molecular Simulations for the Next Decade*, Vol. 605 of *Lecture Notes in Physics*, edited by P. Nielaba, M. Mareschal, and G. Ciccotti, (Springer-Verlag, Berlin, 2002), p. 29, and references therein.
[5] A. Malevanets and R. Kapral, Europhys. Lett. **44**, 552 (1998).
[6] A. Malevanets and R. Kapral, J. Chem. Phys. **110**, 8605 (1999).
[7] T. Ihle, D. M. Kroll, Phys. Rev. E **63**, 020201 (2001); A. Lamura, G. Gompper, T. Ihle, and D. M. Kroll, Europhys. Lett. **56**, 768 (2001); **56**, 319 (2001).
[8] A. Malevanets and R. Kapral, J. Chem. Phys. **112**, 7260 (2000).
[9] A. Malevanets and J. M. Yeomans, Europhys. Lett. **52**, 231 (2000).
[10] Y. Hashimoto, Y. Chen, and H. Ohashi, Comput. Phys. Commun. **129**, 56 (2000); Y. Inoue, Y. Chen, and H. Ohashi, Colloids Surf., A **201**, 297 (2002); T. Sakai, Y. Chen, and H. Ohashi, Phys. Rev. E **65**, 031503 (2002).
[11] M. von Smoluchowski, Ann. Phys. (Leipzig) **48**, 1003 (1915); Phys. Z. **17**, 557 (1916); Z. Phys. Chem. **92**, 129 (1917).
[12] M. Pagitsas and R. Kapral, J. Chem. Phys. **69**, 2811 (1978).
[13] S. Lee and M. Karplus, J. Chem. Phys. **86**, 1883 (1987).
[14] N. Agmon and A. Szabo, J. Chem. Phys. **92**, 5270 (1990).
[15] W. Naumann and A. Molski, J. Chem. Phys. **103**, 3474 (1995).
[16] I. V. Gopich and A. I. Burshtein, J. Chem. Phys. **109**, 2833 (1998).
[17] M. Yang, S. Lee, and K. J. Shin, J. Chem. Phys. **108**, 8557 (1998).
[18] I. V. Gopich, A. A. Ovchinnikov, and A. Szabo, Phys. Rev. Lett. **86**, 922 (2001).
[19] H. Kim, M. Yang, and K. J. Shin, J. Chem. Phys. **111**, 1068 (1999).
[20] C. Oh, H. Kim, and K. J. Shin, J. Chem. Phys. **117**, 3269 (2002).
[21] A. V. Popov and N. Agmon, J. Chem. Phys. **115**, 8921 (2001).
[22] A. V. Popov and N. Agmon, J. Chem. Phys. **118**, 11057 (2003).
[23] B. U. Felderhof and J. M. Deutch, J. Chem. Phys. **64**, 4551 (1976).
[24] J. Lebenhaft and R. Kapral, J. Stat. Phys. **20**, 25 (1979).
[25] B. U. Felderhof, J. M. Deutch, and U. M. Titulaer, J. Chem. Phys. **76**, 4178 (1982).
[26] B. U. Felderhof and R. B. Jones, J. Chem. Phys. **103**, 10 201 (1995).
[27] I. V. Gopich, A. A. Kipriyanov, and A. B. Doktorov, J. Chem. Phys. **110**, 10888 (1999).
[28] B. U. Felderhof and R. B. Jones, J. Chem. Phys. **111**, 4205 (1999).

[29] I. V. Gopich, A. M. Berezhkovskii, and A. Szabo, J. Chem. Phys. **117**, 2987 (2002).
[30] A. Malevanets and R. Kapral, in *Novel Methods in Soft Matter Simulations*, edited by M. Karttunen, I. Vattulainen, and A. Lukkarinen, (Springer-Verlag, Berlin, 2003), p. 113.
[31] G. A. Bird, *Molecular Gas Dynamics* (Clarendon, Oxford, 1976); G. A. Bird, Comput. Math. Appl. **35**, 1 (1998).
[32] H. Mori, Prog. Theor. Phys. **33**, 423 (1965).
[33] F. C. Collins and G. E. Kimball, J. Colloid Sci. **4**, 425 (1949).
[34] R. Kapral, Adv. Chem. Phys. **48**, 71 (1981).